Available online at www.sciencedirect.com
SCIENCE DIRECT®
Journal of Molecular Catalysis A: Chemical 231 (2005) 181–189
JOURNAL OF MOLECULAR CATALYSIS A: CHEMICAL
www.elsevier.com/locate/molcata

PIO study on 1,3-butanediol dehydration over CeO_2 (1 1 1) surface

Naoki Ichikawa[a], Satoshi Sato[b,*], Ryoji Takahashi[b], Toshiaki Sodesawa[b]

[a] *Graduate School of Science and Technology, Chiba University, Yayoi, Inage, Chiba 263-8522, Japan*
[b] *Department of Applied Chemistry, Faculty of Engineering, Chiba University, Yayoi, Inage, Chiba 263-8522, Japan*

Received 30 November 2004; received in revised form 4 January 2005; accepted 4 January 2005

Abstract

CeO_2 has specific catalytic activity for the selective dehydration of 1,3-diols to unsaturated alcohols. In order to clarify the catalytic mechanism, quantum calculation based on the paired interacting orbital (PIO) theory was adopted to 1,3-butanediol–Ce_9O_{18} cluster systems. Strong attractive interaction was observed between 1,3-butanediol and oxygen-defected CeO_2 (1 1 1), where three in-phase interactions were confirmed between H atom at 2-position in 1,3-butanediol and Ce cation and between two OH groups and other Ce cations. In addition, out-of-phase interaction between H and C atom at 2-position was induced by the in-phase interaction between H atom and Ce cation at appropriate coordinate of 1,3-butanediol. The PIO results suggest that the dehydration of 1,3-diols initiates from the abstraction of H atom at 2-position in 1,3-butanediol adsorbed on an oxygen defect site on CeO_2 (1 1 1) with tridentate coordination.

Keywords: CeO_2; Redox property; 1,3-Diol; Dehydration; Unsaturated alcohols; Paired interacting orbital (PIO) theory

1. Introduction

Recently, we have found attractive reactions for synthesizing unsaturated alcohols through the selective dehydration of diols over CeO_2 [1–3]. For example, 1,3-butanediol is dehydrated at 325 °C with the conversion of 36.9% into 3-buten-2-ol and *trans*-2-buten-1-ol with the selectivity of 56.9 and 35.5 mol%, respectively [2], while 3-buten-1-ol, *cis*-2-buten-1-ol and fully dehydrated 1,3-butadiene are rarely formed during the reaction. 1,4-Butanediol is also dehydrated into 3-buten-1-ol over CeO_2 at 400 °C [3].

Dehydration of alcohols readily proceeds over acid and base catalysts [4]. In the acid- and base-catalyzed dehydration of alcohols, reaction should proceed via E1 or E2 and E1cB mechanism, respectively. Hence, the dehydration of 1,3-butanediol over acid and base would produce 2-buten-1-ol (Sayzeff elimination product) and 3-buten-1-ol (Hoffmann elimination product), respectively. These products did not match the reaction results: 3-buten-2-ol and *trans*-2-buten-1-ol were major products over CeO_2. Therefore, we have concluded that both the redox property of CeO_2 and the molecular structure of 1,3-diols would be significant in the dehydration [2].

We speculate the reaction mechanism of the dehydration of 1,3-diols to unsaturated alcohols over CeO_2 as follows (Fig. 5 in Ref. [2]): initially, an H atom at 2-position in methylene group and two OH groups in 1,3-diol coordinate Ce cations. Then, the H atom is withdrawn by Ce^{4+} cation as a radical, and H radical donates one electron to reduce Ce^{4+} to Ce^{3+}, then the H radical itself is oxidized to proton. Finally, an OH group is radically abstracted to yield allylic alcohols, and OH radical and proton recombined to H_2O with abstracting one electron from Ce^{3+} to yield Ce^{4+}. Although the mechanism well explains the dehydration of diols over CeO_2, it is difficult to experimentally prove that the mechanism is correct.

Paired interacting orbital (PIO) [5,6] theory has made successful results in analyzing the mechanisms of ethylene polymerization over Ziegler–Natta catalysts [7–9], Beckmann rearrangement of cyclohexanone oxime over ZSM-5 [10] and acid-catalyzed transformation of rubrene to indenonaphthacene [11]. In this work, the quantum calculation based on PIO theory is employed to compre-

* Corresponding author. Tel.: +81 43 290 3376; fax: +81 43 290 3401.
E-mail address: satoshi@faculty.chiba-u.jp (S. Sato).

1381-1169/$ – see front matter © 2005 Elsevier B.V. All rights reserved.
doi:10.1016/j.molcata.2005.01.017

hend the interaction between CeO_2 surface and 1,3-butanediol.

CeO_2 (1 1 1) surface, as shown in Fig. 1a, is known as the most stable surface among low-index planes of CeO_2 [12,13], and outermost surface of CeO_2 (1 1 1) is terminated with oxygen. In the proposed mechanism [2], three exposed Ce cations should be introduced on CeO_2 surface to interact with 1,3-butanediol. Several research groups observed the oxygen defects introduced on CeO_2 (1 1 1) surface with annealing under high vacuuming condition and the triangular Ce cations being exposed at the defect site by STM [14,15] and non-contact AFM [16,17]. Therefore, we employ an oxygen-defected CeO_2 (1 1 1) surface and discuss the validity of the mechanism mentioned above.

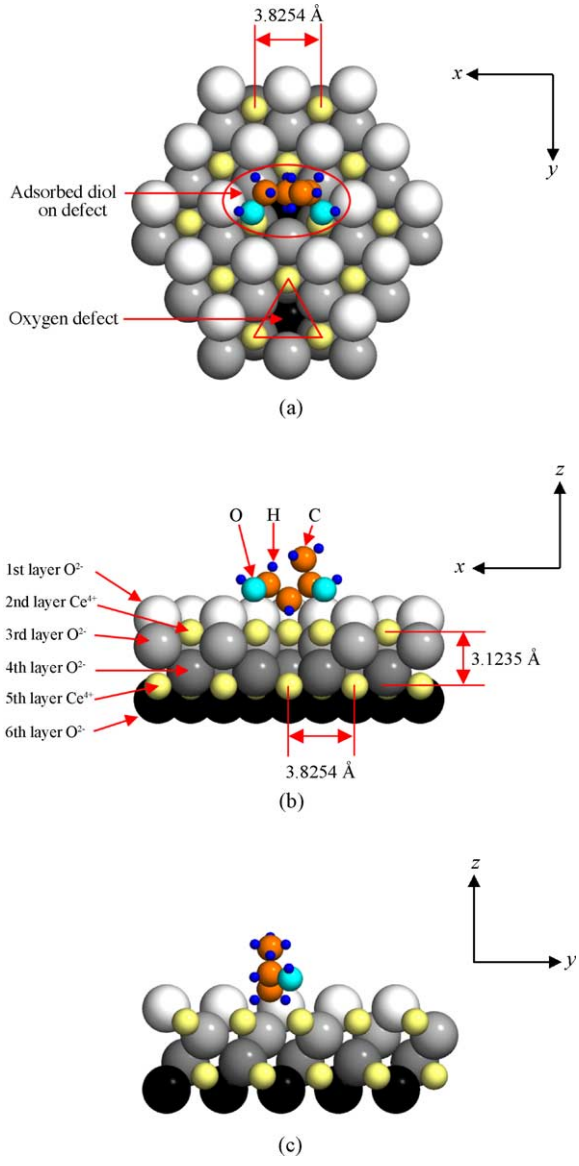

Fig. 1. Adsorption model of 1,3-butanediol on oxygen defect site of CeO_2 (1 1 1). (a) Top view, (b) side view from the bottom of (a), and (c) side view from the right of (a).

2. Experimental

We built CeO_2 (1 1 1) surface and 1,3-butanediol molecular, according to the adsorption model [2]. Fig. 1 depicts the probable adsorption model, in which 2-position H atom and two O atoms in OH groups in 1,3-butanediol coordinated three-triangular Ce cations on the oxygen defect site of CeO_2 (1 1 1) surface.

For the calculation, we modeled a Ce_9O_{18} cluster, which represented CeO_2 (1 1 1) surface as shown in Fig. 2, with the lattice constant of fluorite, CeO_2, of 5.41 Å. To determine the coordinate of 1,3-butanediol over Ce_9O_{18} cluster, we fixed Ce^2 atom as the origin of the coordinate and defined the *x*-, *y*- and *z*-axes (Fig. 2d). The center of 1,3-butanediol was put on the C^2 atom. In the calculations, *x*-coordinate was fixed at 0, and *y* and *z* varied in the unit of Å.

1,3-Butanediol molecule was modeled with following information: dist(C–C) =1.54 Å, dist(C–O) = 1.43 Å, dist(C–H) = 1.09 Å, dist(O–H) = 0.96 Å, ang(C–C–C) = ang(O–C–C) = ang(H–C–C) = 109.5°, and ang(H–O–C) = 104.5°, where dist and ang are abbreviation of distance and angle, respectively.

PIO analysis proposed by Fujimoto et al. [5,6] was executed with LUMMOX^{TM} software system [18]. PIO theory is the method to determine the orbital that plays important roles in chemical interaction between fragments A and B. In this case, A and B were Ce_9O_{18} cluster and 1,3-butanediol, respectively. The molecular orbitals of Ce_9O_{18}, 1,3-butanediol and an interacting system C of the fragments were determined by the extended Hückel theory. We fixed the charge of Ce_9O_{18} cluster and 1,3-butanediol at 0 in this study. The extended Hückel parameters of each atom are listed in Table 1 [19,20]. The algorithm of PIOs is summarized elsewhere [5,7–10]. The eigenvalue of each PIO quantifies the importance of the PIO, and PIOs are labeled as PIO-*n*, where *n* means the sequence of the importance of PIOs. In other words, PIO-1 has the largest eigenvalue and is the most important in all PIOs. Adsorption energy at the state of coordinate can be calculated with the following equation:

$$E_{ad} = E_c - (E_{Ce_9O_{18}} + E_{BDO})$$

Table 1
Extended Hückel parameters for calculation

Atom	Orbital	H_{ij} (eV)	ζ
H[a]	1s	−13.600	1.300
C[a]	2s	−21.400	1.625
	2p	−11.400	1.625
O[a]	2s	−32.300	2.275
	2p	−14.800	2.275
Ce[b]	6s	−4.968	1.398
	5p	−28.613	3.066
	5d	−6.360	1.919

[a] Ref. [19].
[b] Ref. [20].

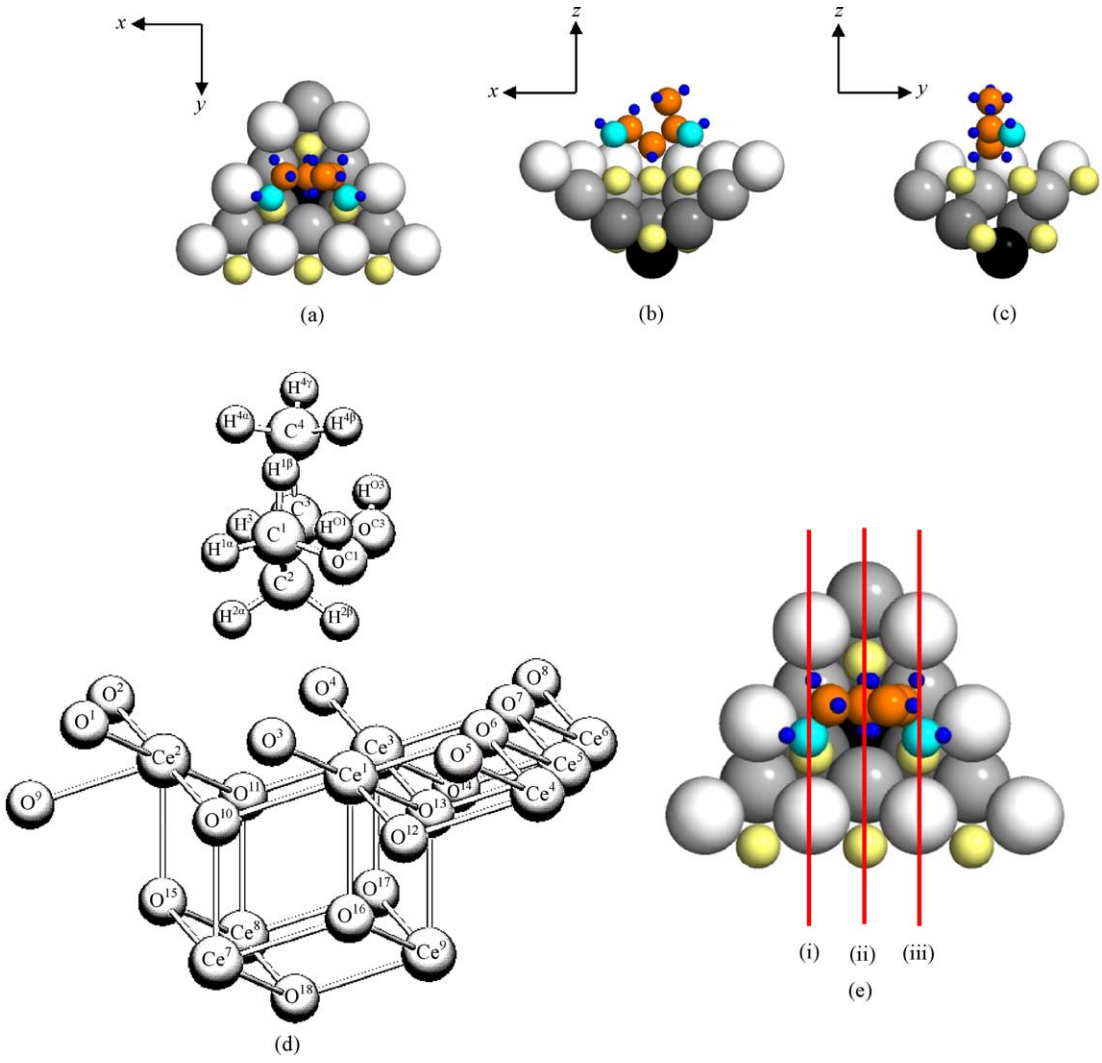

Fig. 2. 1,3-Butanediol–Ce_9O_{18} cluster model. (a) Top view, (b) side view from the bottom of (a), (c) side view from the right of (a), (d) denomination of each atom and (e) cut-out plane to see the interactions between (i) O^{C1} and Ce^1, (ii) methylene group at 2-position (C^2, $H^{2\alpha}$ and $H^{2\beta}$), and (iii) O^{C3} and Ce^3 in Fig. 3.

where E_{ad}, E_c, $E_{Ce_9O_{18}}$, and E_{BDO} are adsorption energy, energy of combined system, that of Ce_9O_{18} cluster, and that of 1,3-butanediol, respectively.

3. Results

Table 2 summarizes a relative adsorption energy, ΔE_{ad}, at various coordinates. ΔE_{ad} was defined as the following equation:

$$\Delta E_{ad} = E_{ad} - E_{ad(y=1.7,z=2.6)}$$

The largest adsorption energy, the smallest ΔE_{ad}, was obtained at the coordinate of $y = 2.1$, $z = 2.4$ with the 1,3-butanediol conformation as shown in Fig. 2. Hereafter, we discussed only the coordinate that allowed the largest adsorption energy at the same height, z, e.g. $y = 2.1$ at

Table 2
ΔE_{ad} at several coordinates[a]

z (Å)	y (Å)						
	1.7	1.8	1.9	2.0	2.1	2.2	2.3
2.6	0	−0.02013	−0.03444	−0.04333	−0.04737	−0.04716	−0.04346
2.5	−0.00419	−0.02784	−0.04457	−0.05483	−0.05923	−0.05849	−0.05352
2.4	−0.00825	−0.03412	−0.05204	−0.06257	−0.06640	−0.06430	−0.05729
2.3	−0.01367	−0.03893	−0.05553	−0.06418	−0.06563	−0.06072	−0.05054
2.2	−0.02146	−0.04159	−0.05271	−0.05588	−0.05203	−0.04200	−0.02697
2.1	−0.03064	−0.03938	−0.03913	−0.03159	−0.01802	0.00041	0.02249

[a] Unit of energy is eV. Underline shows the largest adsorption energy at the same height, z.

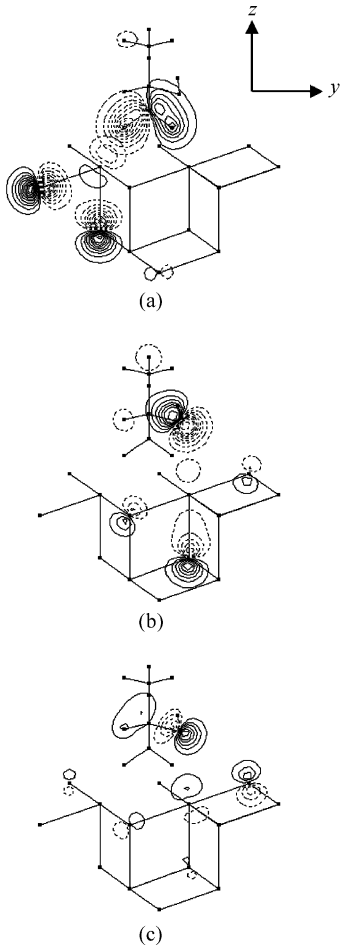

Fig. 3. Counter maps of PIO-1–6 in view of Fig. 2c at the coordinate of $y = 1.8$, $z = 2.1$. (a) PIO-1, on the plane (ii) in Fig. 2e; (b) PIO-2, plane (iii); (c) PIO-3, plane (i); (d) PIO-4, plane (i); (e) PIO-5, plane (ii); and (f) PIO-6, plane (ii).

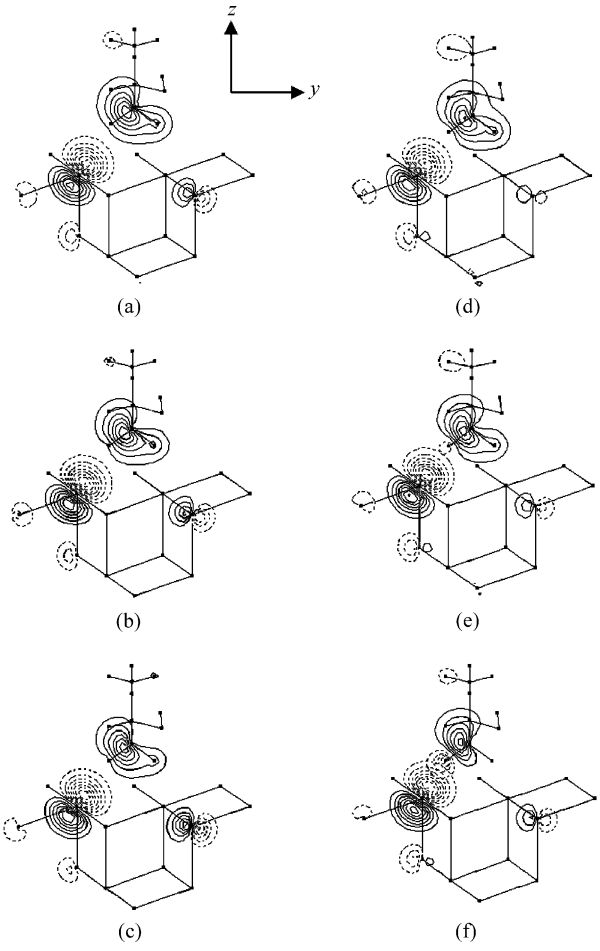

Fig. 4. Counter maps representing the abstraction process of H atom from 1,3-butanediol at several coordinates in view of Fig. 2c on the plane (ii) in Fig. 2e. (a) $y = 2.1$, $z = 2.6$; (b) $y = 2.1$, $z = 2.5$; (c) $y = 2.1$, $z = 2.4$; (d) $y = 2.1$, $z = 2.3$; (e) $y = 2.0$, $z = 2.2$; (f) $y = 1.8$, $z = 2.1$.

$z = 2.6$ and $y = 2.0$ at $z = 2.2$, as shown in the underlines in Table 2.

Fig. 3 shows counter maps of the representative six PIOs coordinate at $y = 1.8$ and $z = 2.1$. Table 3 lists eigenvalues and atomic orbital (AO) components of PIOs at the coordinate. Then, we determined the role of each PIO as follows: PIO-1 showed the in-phase interaction between 2-position H atom and Ce cation, and PIO-2, -3 and -4 showed the in-phase interaction between O atoms in OH groups and Ce cations. PIO-5 showed the out-of-phase interaction between C atom

Table 3
Eigenvalues and LCAO representations of PIO-n (n = 1–6) at the coordinate of $y = 1.8$ and $z = 2.1$.

n	Eigenvalue	Component
1	0.85	$\psi_1 = -0.17\mathrm{Ce}^2_{5pz} - 0.11\mathrm{Ce}^2_{5py} - 0.65\mathrm{O}^9_{2py} - 0.60\mathrm{O}^{15}_{2pz} - 0.14\mathrm{O}^9_{2pz}$ $\varphi_1 = -0.46\mathrm{H}^{2\alpha}_{1s} + 0.46\mathrm{C}^2_{2py} + 0.33\mathrm{H}^{2\beta}_{1s}$
2	0.20	$\psi_2 = +0.26\mathrm{Ce}^3_{5dz2} + 0.19\mathrm{Ce}^3_{6s} - 0.41\mathrm{O}^{16}_{2pz} + 0.36\mathrm{O}^{17}_{2pz} + 0.23\mathrm{O}^{12}_{2px}$ $\varphi_2 = +0.56\mathrm{O}^{C3}_{2py} - 0.44\mathrm{O}^{C3}_{2pz} + 0.40\mathrm{O}^{C1}_{2pz}$
3	0.13	$\psi_3 = -0.15\mathrm{Ce}^1_{6s} - 0.13\mathrm{Ce}^3_{5px} + 0.24\mathrm{O}^{13}_{2py} + 0.22\mathrm{O}^4_{2pz} - 0.21\mathrm{O}^5_{2py}$ $\varphi_3 = -0.38\mathrm{O}^{C3}_{2py} + 0.38\mathrm{C}^2_{2s} - 0.30\mathrm{O}^{C1}_{2py}$
4	0.09	$\psi_4 = -0.40\mathrm{Ce}^1_{5dz2} - 0.28\mathrm{Ce}^3_{6s} - 0.32\mathrm{Ce}^3_{5dz2} + 0.29\mathrm{O}^{13}_{2py} - 0.28\mathrm{O}^3_{2px}$ $\varphi_4 = 0.49\mathrm{O}^{C3}_{2pz} + 0.46\mathrm{O}^{C1}_{2pz} - 0.40\mathrm{O}^{C1}_{2py}$
5	0.09	$\psi_5 = +0.24\mathrm{Ce}^2_{5pz} + 0.18\mathrm{Ce}^2_{5py} - 0.34\mathrm{O}^{14}_{2px} + 0.32\mathrm{O}^4_{2pz} - 0.30\mathrm{O}^{16}_{2pz}$ $\varphi_5 = +0.39\mathrm{C}^2_{2pz} - 0.31\mathrm{H}^{2\beta}_{1s} - 0.27\mathrm{C}^4_{2pz}$
6	0.05	$\psi_6 = +0.53\mathrm{Ce}^2_{5pz} + 0.34\mathrm{Ce}^2_{5py} + 0.28\mathrm{O}^{17}_{2pz} - 0.19\mathrm{O}^{12}_{2px} + 0.19\mathrm{O}^{14}_{2px}$ $\varphi_6 = -0.44\mathrm{C}^2_{2s} + 0.40\mathrm{H}^{2\alpha}_{1s} + 0.36\mathrm{C}^2_{2py}$

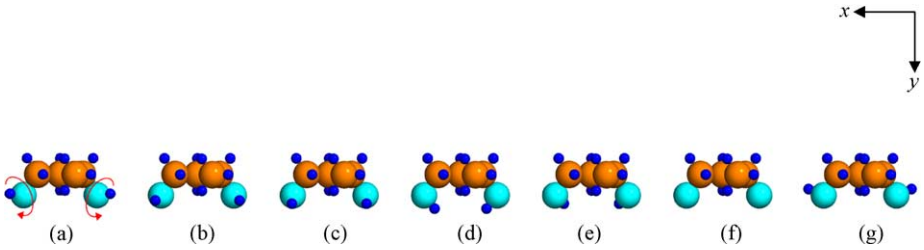

Fig. 5. Top view of 1,3-butanediol with different rotation angle of H^O atoms around O^C—C bonds. (a) 0°, (b) 40°, (c) 60°, (d) 120°, (e) 180°, (f) 240°, and (g) 300°.

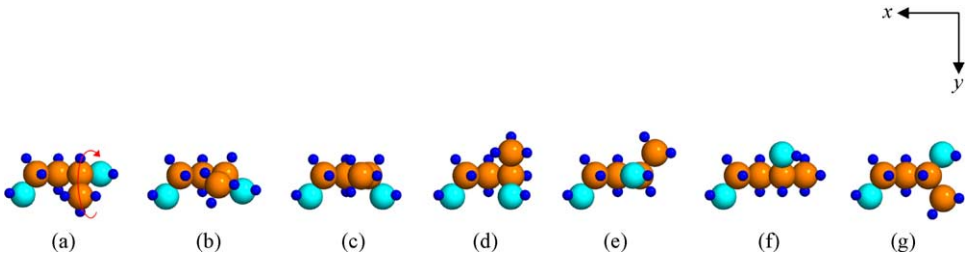

Fig. 6. Top view of 1,3-butanediol with different rotation angle of O^{C3} atom around C^3—C^2 bond. (a) 0°, (b) 40°, (c) 60°, (d) 120°, (e) 180°, (f) 240°, and (g) 300°.

in the methylene group and Ce cation, which probably represents steric hindrance between Ce_9O_{18} cluster surface and 1,3-butanediol. PIO-6 exhibited out-of-phase interaction between H and C atom in methylene group induced by in-phase interaction between the H atom and Ce cation. The PIO-6 obviously indicates the abstraction of H atom at 2-position in 1,3-butanediol by a Ce cation.

Fig. 4 shows counter maps of the PIO that represents the abstraction of H atom at 2-position in 1,3-butanediol (Fig. 3f) at different coordinates. At the most stable coordinate, $y = 2.1$ and $z = 2.4$, no interaction between H atom at 2-position and Ce cation was observed (Fig. 4c). A small interaction was confirmed at the coordinate of $y = 2.0$ and $z = 2.2$ (Fig. 4e). In the closest coordinate, $y = 1.8$ and $z = 2.1$, the interaction increased. The closer 1,3-butanediol approached the Ce_9O_{18} cluster surface, the larger the out-of-phase interaction between H and C atom in methylene group became.

We carried out two series of calculations to confirm the reliable configuration of 1,3-butanediol. One is the effect of rotation of H^O atoms around O^C–C bonds and the other is that of O^{C3} atom around C^3–C^2 bond on the adsorption energy. These atoms were rotated in the manner of being shown in Figs. 5 and 6. Here, we would like to note that all the calculations (Figs. 3 and 4, and Tables 2 and 3) were executed at the fixed rotation angles of $H^O = 0°$ and $O^{C3} = 60°$. Table 4 summarizes the adsorption energy at different rotation angle of H^O atoms, and Fig. 7 shows the change in the molecular energy of 1,3-butanediol and adsorption energy with the rotation angle of H^O atoms. The molecular energy of 1,3-butanediol is roughly constant at any rotation angle of H^O. The largest and the smallest adsorption energies were obtained at the rotation angle of 40 and 250°, respectively (Fig. 7). Table 5 summarizes the adsorption energy at different rotation angle of O^{C3} atom, and Fig. 8 exhibits the change in the molecular energy of 1,3-butanediol and adsorption energy with the rotation angle of O^{C3} atom. The rotational energy barrier of 1,3-butanediol was quite large with rotating O^{C3} atom, which reflected the large substituent at C^3 atom,

Table 4
Adsorption energy of 1,3-butanediol with rotating H_O atoms around O_C—C bonds at the coordinate of $y = 1.8$ and $z = 2.1$[a]

Rotation angle[b]	$E_{Ce_9O_{18}}$	E_{BDO}	E_c	E_{ad}
0	−3517.35	−715.53	−4241.40	−8.52
40	−3517.35	−715.50	−4241.46	−8.61
60	−3517.35	−715.49	−4241.41	−8.57
120	−3517.35	−715.56	−4241.24	−8.33
180	−3517.35	−715.49	−4240.90	−8.06
240	−3517.35	−715.55	−4240.49	−7.59
300	−3517.35	−715.48	−4240.84	−8.01

[a] Unit of energy is eV. Unit of y and z is Å.
[b] Rotation angle (°) was defined as shown in Fig. 5.

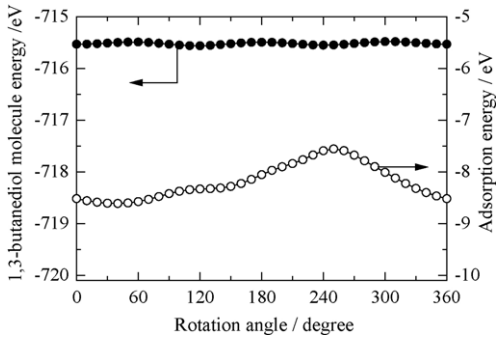

Fig. 7. Energy diagram of the rotation of H^O atoms around O^C—C bonds. Closed circle: 1,3-butanediol molecule energy, open circle: adsorption energy.

Table 5
Adsorption energy of 1,3-butanediol with rotating O_{C3} atom around C_3–C_2 bond at the coordinate of $y = 1.8$ and $z = 2.1$[a]

Rotation angle[b]	$E_{Ce_9O_{18}}$	E_{BDO}	E_c	E_{ad}
0	−3517.35	−716.58	−4242.15	−8.21
40	−3517.35	−715.64	−4241.67	−8.68
60	−3517.35	−715.53	−4241.40	−8.52
120	−3517.35	−716.57	−4241.60	−7.68
180	−3517.35	−716.25	−4241.71	−8.11
240	−3517.35	−716.67	−4240.92	−6.90
300	−3517.35	−716.48	−4241.12	−7.29

[a] Unit of energy is eV. Unit of y and z is Å.
[b] Rotation angle (°) was defined as shown in Fig. 6.

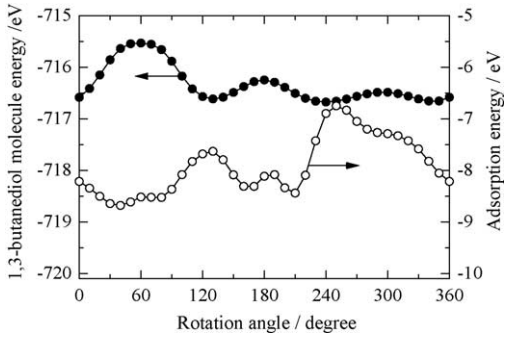

Fig. 8. Energy diagram of the rotation of O^{C3} atom around C^3–C^2 bond. Symbols are the same as those in Fig. 7.

methyl and OH groups. 1,3-Butanediol molecule itself was the most stable at the rotation angle of $O^{C3} = 240°$ within the calculations, while adsorption energy was nearly the smallest. The largest adsorption energy was obtained at the rotation angle of $O^{C3} = 40°$, where two OH groups adsorbed on Ce atoms.

We also carried out calculations to confirm an abstraction model of hydrogen from C–H of 2-position methylene in 1,3-butanediol (Table 6). The calculations were executed in the model in which the coordinate of the carbon atom of the methylene is fixed at $y = 2.1$ and $z = 2.4$ and elongate the C–H bond of the methylene toward the surface Ce cation. It is noticed that the adsorption energy increases with elongating the C–H bond length. Out-of-phase interaction between H and C atom in methylene group was observed at d(C–H)=1.2,

Table 6
Adsorption energy of 1,3-butanediol with different distances of C–H in the 2-position methylene at the coordinate of $y = 2.1$ and $z = 2.4$[a]

d(C–H)[b]	d(Ce–H)[b]	$E_{Ce_9O_{18}}$	E_{BDO}	E_c	E_{ad}
1.09	2.145	−3517.35	−715.53	−4241.43	−8.54
1.10	2.135	−3517.35	−715.51	−4241.40	−8.54
1.20	2.042	−3517.35	−715.26	−4241.18	−8.57
1.30	1.949	−3517.35	−714.98	−4241.00	−8.67
1.40	1.857	−3517.35	−714.67	−4240.87	−8.86
1.50	1.766	−3517.35	−714.34	−4240.84	−9.15
1.60	1.676	−3517.35	−714.02	−4240.91	−9.54
1.70	1.587	−3517.35	−713.70	−4241.06	−10.01

[a] Unit of energy is eV. Unit of y and z is Å.
[b] Distance between the atoms (Å). The Ce–C distance is fixed at 3.189 Å.

in a similar manner as shown in Fig. 4e (figure not shown), and it increases with increasing the C–H bond length, like in Fig. 4f.

Finally, we considered the adsorption for another model of optical isomer of 1,3-butanediol (Fig. 9b). The conformation in Fig. 9a is the same as that of Fig. 2. Then, we calculated the adsorption energy with 1,3-butanediol on Ce_9O_{18} in Fig. 9 at the coordinate of $y = 1.8$ and $z = 2.1$. The adsorption energy of Fig. 9b was smaller than that of Fig. 9a by 0.53 eV.

4. Discussion

4.1. Validity of adsorption model of 1,3-butanediol on CeO_2 (1 1 1) surface

In this study, we assumed the adsorption model (Fig. 1) based on the results of catalytic reaction [2]. We have to discuss and evaluate the adsorption model. The adsorption model explains products selectivity: 1,3-butanediol is dehydrated into 3-buten-2-ol or into 2-buten-1-ol in *trans*-form, while *cis* isomer is rarely obtained in the reaction [1,2]. Fig. 9 depicted the schematic surface dehydration models of 1,3-butanediol into 3-buten-2-ol, *cis*-, and *trans*-2-buten-1-ol. In Fig. 9b, a methyl group in the optical isomer of 1,3-butanediol approached the CeO_2 (1 1 1) surface, and *cis*-2-buten-1-ol could be formed. The adsorption energy corresponding to Fig. 9b is smaller than that of Fig. 9a: the adsorption structure in Fig. 9b is restrained. Since the approach induced large steric hindrance between the methyl group and CeO_2 (1 1 1) surface, the *cis*-isomer could be hardly formed. On the other hand, the *trans*-isomer is readily formed because of less steric hindrance of methyl group, which would be the driving force for the selective formation of *trans*-isomer (Fig. 9a). 3-Buten-2-ol could be produced through both the adsorption models.

It is noticed that stable conformation of a 1,3-butanediol molecule on Ce_9O_{18} cluster gives us significant information. In Fig. 8, a 1,3-butanediol molecule itself is the most stable at the O^{C3} rotation angle of 240° and the second most stable at 350°, which are gauche conformation. Adsorption energy, however, is nearly the smallest at 240° and relatively small at 0°. The largest adsorption energy is obtained at 40°, while the molecule itself is relatively unstable at the conformation. These results imply that 1,3-butanediol molecule is stabilized by the interaction between O atoms of the molecule and surface Ce cations.

Another question is whether the most acidic H atoms in OH groups of 1,3-butanediol are abstracted or not. Adsorption energy is lessened when the H atoms in OH groups approached Ce cations (Table 4). Hence, the interaction between H atoms in OH groups and Ce cations is unfavorable for the adsorption of 1,3-butanediol on an oxygen-defect site of CeO_2 surface. Namely, the acidic H atoms in OH groups of 1,3-butanediol are not abstracted in the model.

In this study, we obtained large values of adsorption energy, ca. 8 eV, which are much larger than usual chemisorp-

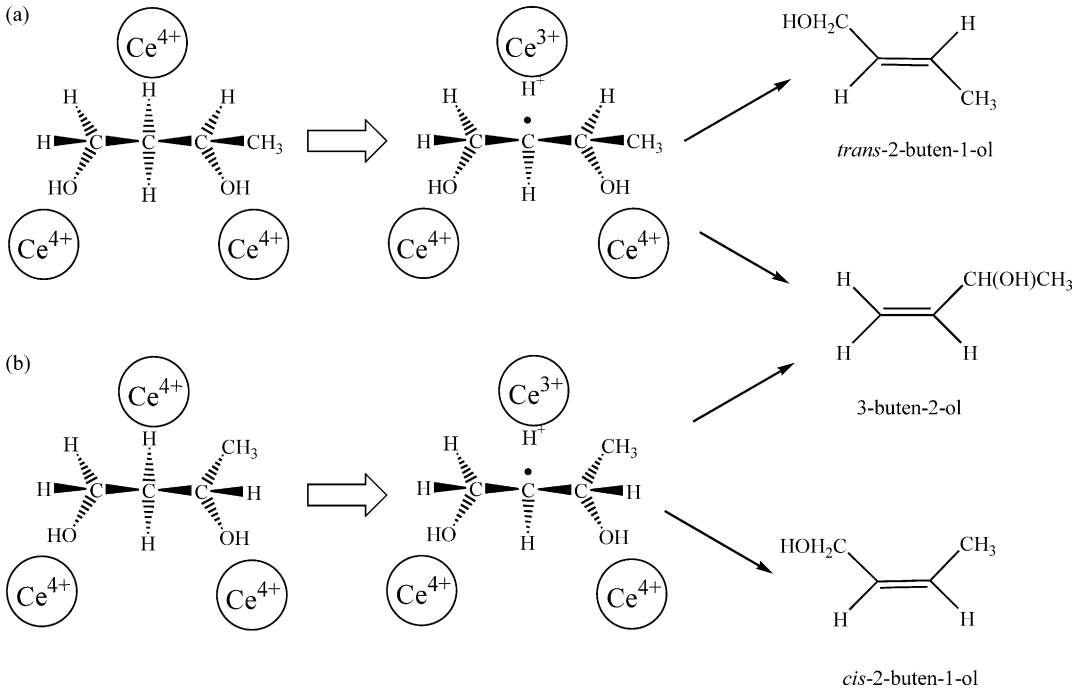

Fig. 9. Top view of schematic reaction mechanism in the dehydration of 1,3-butanediol to (a) *trans*-2-buten-1-ol and (b) *cis*-2-buten-1-ol.

tion energy, ca. 1 eV. Although the large values calculated may be caused by the limitation of using the extended Hückel parameters, we used them in the comparative discussion. In addition, we did not carry out the structural optimization of 1,3-butanediol–Ce_9O_{18} cluster system with the methods such as ab initio and DFT at all. There could be more reliable conformation of 1,3-butanediol on Ce_9O_{18} cluster. The structural optimization will be performed in the near future. However, we would like to emphasis that the calculation results support the proposed adsorption model.

4.2. Interaction between Ce_9O_{18} cluster and 1,3-butanediol

Fig. 3 depicts six significant PIOs of 1,3-butanediol–Ce_9O_{18} system. These PIOs showed good coincidence with our proposed reaction mechanism [2]; PIO-1 represented the coordination of $H^{2\alpha}$ atom to Ce cation, and PIO-2, -3, and -4 showed that of O^C atoms to Ce cations and PIO-6 exhibited the abstraction of $H^{2\alpha}$ atom from methylene group at 2-position of 1,3-butanediol. Out-of-phase interaction between O^C of OH groups and C atoms was not observed at this coordinate, which means that the cleavage of C–OH bond is not the initiation step of dehydration. Hence, $H^{2\alpha}$ atom would be abstracted initially from 1,3-butanediol in the dehydration. In the adsorption of methanol on the ceria single crystal, however, methanol dissociatively adsorbs on oxygen vacancies on the CeO_2 (1 1 1) surface [17]. It is quite interesting that C–H bond cleavage initiates the dehydration of diols. This could be restricted to the adsorption of diols, and will be a target of research in future.

Unfortunately, we are not able to determine whether the abstraction of $H^{2\alpha}$ atom was promoted in the form of radical or ionic species with the calculation results. CeO_2 had only weak basic sites on its surface without acidic sites [21]. If the basic sites activate H atoms, a more acidic H in OH groups should be abstracted. Since the dehydration of 1,3-diols to unsaturated alcohols proceeds only over CeO_2 [1,2], it is reasonable that redox property of CeO_2 probably promoted the abstraction of $H^{2\alpha}$ atom. While 1,3-butanediol was the most stabilized at the coordinate of $y = 2.1$, $z = 2.4$ (Table 2), the abstraction process of $H^{2\alpha}$ atom is not observed. At the more closed conformation, the out-of-phase interaction between Ce cation and C^2 atom is confirmed: the abstraction of $H^{2\alpha}$ atom from methylene group at 2-position appears at the coordinate of $y = 2.0$, $z = 2.2$ (Fig. 4e) and it becomes clearer at the coordinate of $y = 1.8$, $z = 2.1$ (Fig. 4f). These results imply that 1,3-butanediol molecule needs to approach Ce cations to be further activated. Table 6 also supports the proposed mechanism; abstraction of H from the methylene group at 2-position stabilizes the adsorption structure.

In this study, we executed all calculations under the conditions that the charge of Ce_9O_{18} cluster was 0. However, Fukui et al. reported that CeO_2 surface was reduced when oxygen defects were produced with annealing under high vacuum conditions because an O anion donated two electrons on the surface to reduce two Ce^{4+} to Ce^{3+} [16,17]. In this sense, we may calculate with the charge of Ce_9O_{18} cluster being −2.

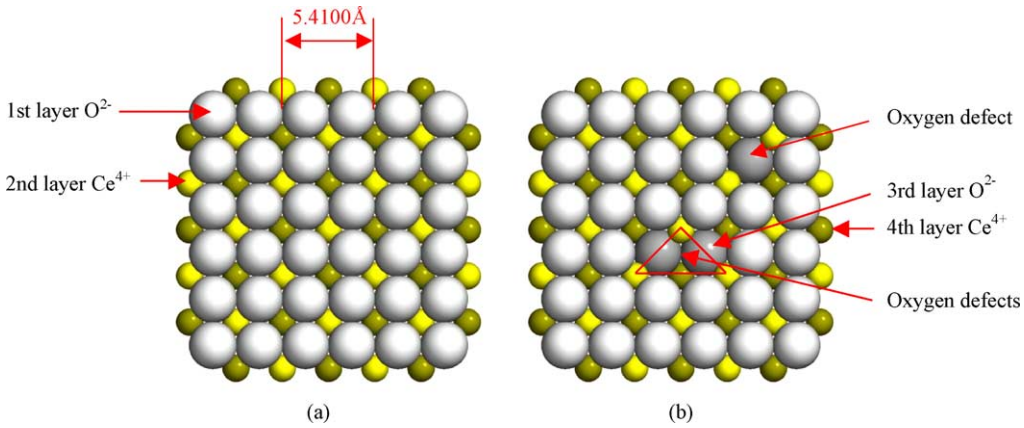

Fig. 10. Images of CeO_2 (1 0 0) surface. (a) Stoichiometric surface, (b) oxygen-defected surface.

When we calculated with the charge of −2, there was no significant difference (data not shown). In the previous report, we proved that water vapor oxidized surface Ce^{3+} to Ce^{4+} at around 300 °C [2]. Thus, most of surface Ce cations probably existed as Ce^{4+} because the dehydration was mainly carried out over 300 °C.

4.3. *Prediction of the activity of CeO_2 (1 0 0) surface with modeling its surface structure*

While it is said that (1 1 1) surface is the most stable among the low-index plane [12,13], several planes with other Miller indexes should be exposed on the CeO_2 surface. Then, we consider (1 0 0) surface with oxygen defects and predict the activity of the surface. Fig. 10a shows the CeO_2 (1 0 0) surface image modeled with simple cleavage of crystal. Conesa [13] has reported that such (1 0 0) surface is unstable and insists that half of the top oxygen anion layer should be removed and relaxation of the top layer occurs to maintain the net zero dipole. Additionally, we would like to note another possibility that the oxygen anion layer may be compensated with hydrogen for the requirement of zero dipole. In this work, we adopted the latter possibility because it is hard to predict the real surface structure after the relaxation of outermost oxygen anion layer. Here, it should be noted that the compensated hydrogens are neglected in Fig. 10a because of simplification.

Fig. 10b shows the possible surface image of CeO_2 (1 0 0) after the introduction of oxygen defects. An oxygen defect is readily formed *via* dehydration of two OH groups. As can be seen in Fig. 10b, two neighboring oxygens should be removed from the surface to expose triangular Ce cations. In Fig. 10a, we can understand that a surface Ce^{4+} cation on the second layer of (1 0 0) plane has 8-coordination. In contrast, a Ce^{4+} cation on the second layer of (1 1 1) plane is 7-coordinated to three 3-fold O^{2-} anions on the top layer and four 4-fold O^{2-} in the third-layer (Fig. 1). Thus, three Ce^{4+} cations on the oxygen defect of (1 1 1) plane have the coordination number of 6, while two Ce^{4+} cations have 7 and one Ce^{4+} cation has 6 on two-oxygen-defect site of the (1 0 0) plane. Hence, it is speculated that surface of (1 1 1) plane is more active than that of (1 0 0) plane. Practically, a difference in catalytic activity between (1 1 1) and (1 0 0) crystal planes of CeO_2 has been reported: propanone is formed only on the (1 1 1) plane in the ketonization of acetic acid [22]. The CeO_2 (1 0 0) plane dose not catalyze the ketonization. In addition, the distance between Ce^{4+} cations on the surface may affect the activity: the distance on (1 0 0) is much longer than on (1 1 1) as shown in Fig. 10. Therefore, we speculate that CeO_2 (1 1 1) plane is probably the active surface.

5. Conclusion

We executed quantum calculations for the assumed adsorption model of 1,3-butanediol on defected CeO_2 (1 1 1) surface. PIO analysis shows in-phase interactions between a H atom at 2-position and a Ce cation and between two OH groups in 1,3-diol and triangular-Ce cations, and out-of-phase interaction between H and C atoms in the methylene group at 2-position induced by the in-phase interaction between the H atom and Ce cation. These results supports the redox mechanism we proposed. In the initial step, a 2-position H atom and two OH groups in 1,3-diol coordinate triangular-Ce cations exposed on oxygen defect of CeO_2 (1 1 1) surface. Then, the 2-position H atom is withdrawn by Ce^{4+} cation.

References

[1] S. Sato, R. Takahashi, T. Sodesawa, N. Honda, H. Shimizu, Catal. Commun. 4 (2003) 77–81.
[2] S. Sato, R. Takahashi, T. Sodesawa, N. Honda, J. Mol. Catal. A 221 (2004) 177–183.
[3] S. Sato, R. Takahashi, T. Sodesawa, N. Yamamoto, Catal. Commun. 5 (2004) 397–400.
[4] K. Tanabe, M. Misono, Y. Ono, H. Hattori, New Solid Acids and Bases, Kodansha, 1989, pp. 260–267.
[5] H. Fujimoto, N. Koga, K. Fukui, J. Am. Chem. Soc. 103 (1981) 7452–7457.
[6] H. Fujimoto, Acc. Chem. Res. 20 (1987) 448–453.

[7] A. Shiga, H. Kawamura-Kuribayashi, T. Sasaki, J. Mol. Catal. 87 (1994) 243–261.
[8] A. Shiga, H. Kawamura-Kuribayashi, T. Sasaki, J. Mol. Catal. A 98 (1995) 15–24.
[9] A. Shiga, J. Mol. Catal. A 146 (1999) 325–334.
[10] M. Ishida, T. Suzuki, H. Ichihashi, A. Shiga, Catal. Today 87 (2003) 187–194.
[11] T. Hosokawa, H. Nakano, K. Takami, K. Kobiro, A. Shiga, Tetrahedron Lett. 44 (2003) 1175–1177.
[12] T.X.T. Sayle, S.C. Parker, C.R.A. Catlow, Surf. Sci. 316 (1994) 329–336.
[13] J.C. Conesa, Surf. Sci. 339 (1995) 337–352.
[14] H. Nörenberg, G.A.D. Briggs, Surf. Sci. 402–404 (1998) 734–737.
[15] H. Nörenberg, G.A.D. Briggs, Surf. Sci. 424 (1999) L352–L355.
[16] K. Fukui, Y. Namai, Y. Iwasawa, Appl. Surf. Sci. 188 (2002) 252–256.
[17] Y. Namai, K. Fukui, Y. Iwasawa, Catal. Today 85 (2003) 79–91.
[18] T. Motoki, A. Shiga, J. Comput. Chem. 25 (2004) 106–111.
[19] G. Burns, J. Chem. Phys. 41 (1964) 1521–1522.
[20] P. Pyykkö, L.L. Lohr Jr., Inorg. Chem. 20 (1981) 1950–1959.
[21] S. Sato, K. Koizumi, F. Nozaki, J. Catal. 178 (1998) 264–274.
[22] J. Stubenrauch, E. Brosha, J.M. Vohs, Catal. Today 28 (1996) 431–441.